Environmental Fluid Mechanics (2006) 6: 181–202
DOI 10.1007/s10652-005-5656-9

Evaluation of CFD Simulation using RANS Turbulence Models for Building Effects on Pollutant Dispersion

XIN WANG[a,*] and KEVIN F. McNAMARA[b]
[a]*Department of Civil Engineering, Faculty of Construction, Guangdong University of Technology, 729 East Dongfeng Road, Guangzhou, 510090, Guangdong, P.R. China,*
[b]*Department of Civil Engineering, National University of Ireland, Galway, Ireland*

Received 2 October 2005; accepted in revised form 5 December 2005

Abstract. CFD evaluations were performed to examine the applicability of the RANS methods in simulating pollutant dispersion near, within and over three typical building configurations: (1) an isolated building, (2) a building array and (3) an urban intersection. The CFD results are compared with values obtained from wind tunnel tests. In some situations major differences between the wind tunnel tests and the CFD results were observed. The main source of difference between the CFD and wind tunnel results was inadequate modelling of local flow patterns using the RANS turbulence models. Also inappropriate evaluation of high intermittent turbulent mixing in the RANS approach may lead to either over-prediction or under-prediction of the concentration level, by up to a factor of 10, depending on the case investigated.

Key words: building effects, CFD evaluation, pollutant dispersion, RANS methods, wind tunnel experiment

1. Introduction

In an urban environment, the transport and dispersion of pollutants, for near-field emission, is directly affected by the aerodynamics of buildings and thus is highly site dependent. Traditionally, information on the near-field concentrations was obtained using physical simulations such as wind-tunnel experiments. Recently, developments in Computational Fluid Dynamics (CFD) make possible an alternative tool to predict concentration fields near buildings. In fact, CFD techniques have been widely used to investigate a diversity of building-effects problems [1–5]. The Reynolds Averaged Navier–Stokes equation (RANS) methods, in which one of the turbulence models supplies the additional equation to solve the correlations of turbulent velocities, are amongst the favourite procedures used to model

*Corresponding author, E-mail: sida_wang@hotmail.com

most urban dispersion problems, mainly due to their inexpensive computational costs. However, comparisons of the RANS results with wind tunnel data show that significant errors could occur in the prediction of concentrations within the aerodynamic footprint of buildings [6, 7]. These errors could come from any inappropriate application of the turbulence model, numerical schemes, grid density and so on [8, 9]. On the other hand, the inherent inconsistencies of the simple eddy-diffusivity model with realistic atmospheric dispersion may also be one of the important sources of error.

This paper presents an evaluation of RANS simulation in a few typical building effects scenarios by comparison with wind tunnel experiment results. Three turbulence models, i.e. the k–ε model, Shear Stress Transport model (SST) and the Speziale–Sarkar–Gatski Reynolds-stress model (SSG), were tested. In order to focus the investigation on the prediction error caused by the turbulence models and by the eddy-diffusivity assumption, a preliminary CFD investigation was conducted to ensure simulation independence of the grid density and numerical schemes [10]. The content of this paper is outlined as follows: the Reynolds averaged governing equation system is given in Section 2, the case details and a brief description of CFD simulation and wind tunnel experiments are demonstrated in Section 3, the corresponding analysis and comparisons are shown in Section 4 and the conclusions are given in Section 5.

2. Reynolds Averaged Governing Equations

For incompressible flows, under the conditions of non-buoyant force and no heat transfer, the Reynolds averaged equations, which govern flow motion and transport and dispersion of pollutants, in tensor notation, are [11]:

$$\text{Conservation of mass}: \frac{\partial U_i}{\partial x_i} = 0 \tag{1}$$

Averaged Navier–Stokes equations:

$$\frac{\partial U_i}{\partial t} + U_j \frac{\partial U_i}{\partial x_j} = \frac{1}{\rho}\frac{\partial P}{\partial x_i} + \frac{\partial}{\partial x_j}\left(\nu \frac{\partial U_i}{\partial x_j} - \overline{u_i' u_j'}\right) \tag{2}$$

$$\text{Pollutant transport equation}: \frac{\partial C}{\partial t} + U_i \frac{\partial C}{\partial x_i} = \frac{\partial}{\partial x_i}\left(D\frac{\partial C}{\partial x_i} - \overline{u_i' c'}\right) + S_\text{p} \tag{3}$$

where x_i are the Cartesian coordinates, t is the time, ρ is the air density and ν is the kinetic viscosity. U_i, P and C are the ith mean velocity

component, mean static pressure and mean pollutant concentration, respectively. u_i', u_j' and c' are the fluctuating components of velocity and pollutant around their means, $\overline{u_i'u_j'}$ is the Reynolds stress tensor and $\overline{u_i'c'}$ is the turbulent pollutant flux, D is the molecular diffusivity and S_p is the volumetric source generation rate of the pollutants.

Due to new unknown correlations, (i.e., $\overline{u_i'u_j'}$ and $u_i'c'$), being introduced into the governing equation system in the Reynolds averaging process, one of the turbulence models has to be used to make the above governing equation system form a closed set. These turbulence models can be categorized as the eddy viscosity based turbulence model and the Reynolds-stress turbulence model.

2.1. EDDY VISCOSITY BASED TURBULENCE MODELS

In the eddy viscosity based turbulence models the unknown turbulent fluxes, $\overline{u_i'u_j'}$, are assumed to be proportional to the strain rate, analogous to its counterpart of viscous shear stress, i.e.

$$-\overline{u_i'u_j'} = \nu_t \left(\frac{\partial U_i}{\partial x_j} + \frac{\partial U_j}{\partial x_i} \right) - \frac{2}{3}\delta_{ij}k \tag{4}$$

where ν_t is the eddy viscosity, δ_{ij} is a Kronecker delta function, and k is the turbulent kinetic energy which is defined by $k = 0.5\overline{u_i'u_i'}$.

The eddy viscosity ν_t is assumed to be proportional to a velocity scale V and a length scale L, i.e.

$$\nu_t \propto VL \tag{5}$$

Based on dimensional analysis V can be characterized using $\sqrt{k}$ and L can be characterized by the large-scale turbulence motion. In practical application there exist several choices associated the length scale L with a specified turbulent quantity. This leads to a number of two-equation turbulence models being suggested. Amongst them, the k–ε based turbulence models relate the length scale L to turbulent kinetic energy dissipation rate ε and the k–ω based turbulence models associate the length scale L with the turbulence frequency ω, i.e.:

$$\nu_t = C_\mu k^2/\varepsilon \quad \text{for the } k-\varepsilon \text{ based turbulence model} \tag{6a}$$

$$\nu_t = k/\omega \quad \text{for the } k-\omega \text{ based turbulence model} \tag{6b}$$

where C_μ is an empirical constant, usually taken as 0.09, the values of k and ε in the standard k–ε turbulence model and k and ω in the k-ω turbulence model are determined by their transport equation individually.

The standard k–ε model is robust and of reasonable accuracy for a large range of flows, but it tends to over-predict the eddy viscosity and thus may

fail to predict flow separation on boundary surfaces [12]. Comparatively, the k–ω model performs better in the near-wall area but it is sensitive to the free-stream boundary. Combination of the advantages of both models in the near-wall region and outside the boundary layer leads to the Shear Stress Transport (SST) model being suggested by Menter [13], in which a limiter to the formulation of eddy viscosity is used to evaluate the proper transport behavior of turbulent shear stress and a blending function is used to transit between the k–ω model and the k–ε model based on the distance to the nearest surface and on the flow variables.

With the eddy viscosity, ν_t, solved, the unknown turbulent pollutant fluxes, $\overline{u_i' c'}$, can be assumed to be proportional to the local gradient of mean concentration:

$$-\overline{u_i' c'} = \frac{\nu_t}{\sigma_c} \frac{\partial C}{\partial x_i} \tag{7}$$

where ν_t/σ_c is the eddy diffusivity, σ_c is the turbulent Schmidt number and roughly equal to a constant of 0.7.

2.2. REYNOLDS-STRESS MODEL [11, 13]

The Reynolds stress model is based on the transport equation of Reynolds stress $-\overline{u_i' u_j'}$ and the ε-equation. By modelling the correlation of turbulence velocities of higher order, the transport equation of Reynolds stress $-\overline{u_i' u_j'}$ is given by:

$$\frac{\partial \overline{u_i' u_j'}}{\partial t} + U_k \frac{\partial \overline{u_i' u_j'}}{\partial x_k} = P_{ij} + \phi_{ij} + \frac{\partial}{\partial_k} \left[\left(\nu + \frac{2}{3} C_s \frac{k^2}{\varepsilon} \right) \frac{\partial \overline{u_i' u_j'}}{\partial x_k} \right] - \frac{2}{3} \delta_{ij} \varepsilon \tag{8}$$

where P_{ij} is the production term of Reynolds stress and ϕ_{ij} is the pressure–strain correlation. They are defined as the follows:

$$P_{ij} = -\left\{ \overline{u_i' u_k'} \frac{\partial U_j}{\partial x_k} + \overline{u_j' u_k'} \frac{\partial U_i}{\partial x_k} \right\} \tag{9}$$

$$\begin{aligned} \phi_{ij} = & -\varepsilon \left\{ C_{s1} a_{ij} + C_{s2} \left(a_{ik} a_{kj} - \frac{1}{3} a_{ij} a_{ij} \delta_{ij} \right) \right\} - C_{r1} P_{ik} a_{kj} + C_{r2} k S_{ij} \\ & - C_{r3} k S_{ij} \sqrt{a_{ij} a_{ij}} + C_{r4k} \left(a_{ik} S_{jk} + S_{ik} a_{jk} - \frac{2}{3} a_{ij} S_{ij} \delta_{ij} \right) \\ & + C_{r5} k \left(a_{ik} W_{jk} + W_{ik} a_{jk} \right) \end{aligned} \tag{10}$$

where a_{ij} is the anisotropic tensor, S_{ij} is the strain rate and W_{ij} is the vorticity. These are given by:

$$a_{ij} = \frac{\overline{u_i' u_j'}}{k} - \frac{2}{3}\delta_{ij}, \quad S_{ij} = \frac{1}{2}\left(\frac{\partial U_i}{\partial x_j} + \frac{\partial U_j}{\partial x_i}\right) \quad \text{and} \quad W_{ij} = \frac{1}{2}\left(\frac{\partial U_i}{\partial x_j} - \frac{\partial U_j}{\partial x_i}\right) \tag{11}$$

The ε-equation reads:

$$\frac{\partial \varepsilon}{\partial t} + U_j \frac{\partial \varepsilon}{\partial x_j} = \frac{\varepsilon}{k}(C_{\varepsilon 1} P_k - C_{\varepsilon 2}\varepsilon) + \frac{\partial}{\partial x_j}\left[\frac{1}{\sigma_{\varepsilon RS}}\left(\nu + C_{\mu RS}\frac{k^2}{\varepsilon}\right)\frac{\partial \varepsilon}{\partial x_k}\right] \tag{12}$$

The modeling of the pressure–strain and dissipation-rate terms constitutes a number of RSM models. Amongst them, the SSG model uses a quadratic relationship for the pressure–strain correlation, the model constants are listed as: $C_{\mu RS} = 0.1, \sigma_{\varepsilon RS} = 1.36, C_s = 0.22, C_{\varepsilon 1} = 1.45$, $C_{\varepsilon 2} = 1.83, C_{s1} = 1.7, C_{s2} = -1.05, C_{r1} = 0.9, C_{r2} = 0.8, C_{r3} = 0.65, C_{r4} = 0.625$ and $C_{r5} = 0.2$ [13]. It should be noted that the turbulent kinetic energy k here is not an independent variable and can be obtained from the principle Reynolds stress components, i.e. $k = 0.5\overline{u_i' u_i'}$.

3. Wind Tunnel Experiment CFD Simulation

3.1. CASE INVESTIGATED

To predict flow and dispersion phenomena in a complex urban environment, it is necessary to simplify the realistic building configurations to some typical building configurations of regular shape and layout. In this evaluation, the cases investigated are for emission from a point source around/above/within an isolated building with different aspect ratios, a 5 by 5 building array with in-line arrangement and an urban intersection with orthogonal layout and an oblique upwind street. The model geometry, source location, coordinate system and concentration receptors, for each case used in this evaluation, are shown in Figures 1–3, respectively. The details of building configurations and source arrangement are also summarized in Table I, (where H, W and L are the building height, width and length, respectively).

3.2. WIND TUNNEL DISPERSION EXPERIMENTS

The wind tunnel experiment was conducted in the boundary layer wind tunnel at the Department of Civil Engineering, National University of Ireland, Galway, which is a low speed, open-return and open working section type wind tunnel. The test section is 1.99 m high, 2.44 m wide and

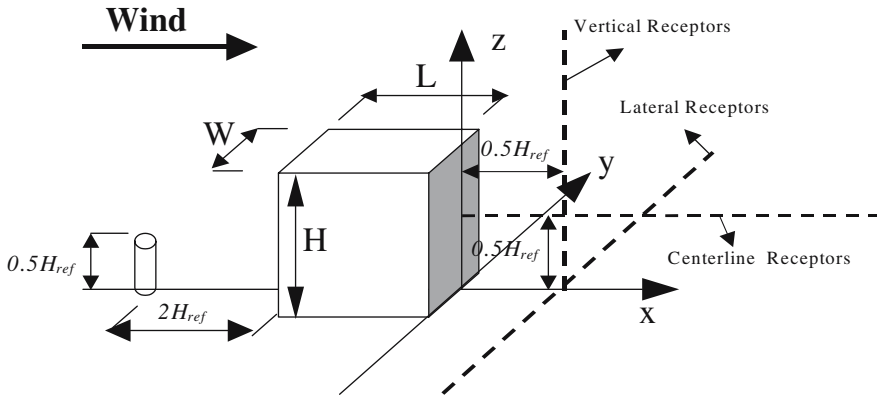

Figure 1. Model, receptors and coordinate system for the isolated building case.

9.9 m long. The wind speed range is 0–7 m/s. Using Irwin-spires, perforated strip and roughness elements with a staggered arrangement a wind-tunnel boundary layer was modelled, which at the experimental site was about 1.0 m thick, the roughness length z_0 was 1.27 mm and the exponent of the power-law velocity profile was 0.256. Based on detailed flow measurements and a comparison with ESDU full-scale data given in references [14–16], the boundary layer represents the roughness terrain for the center of small town at a scale factor of 1:250 [10]. The same scaling factor was used for the relationship between prototypes and models in both the wind tunnel experiments and the numerical simulation. Typically, the model dimensions for Case 1 represents a cubical building of 25 m height.

A Pitot tube was located in front of the test obstacle at a height of 1.0 m. The mean velocity at this height was set to 5.0 m/s and thus the reference wind velocity, U_{ref}, was 2.66 m/s at the reference height of $H_{\text{ref}} = 0.1$ m. The turbulence intensity was 26.4% at the reference height. The friction velocity, u^*, was estimated by fitting the logarithmic law giving a value of 0.245 m/s. The minimum Reynolds number based on the reference height, which represents the minimum building dimension for all cases, was about 1.8×10^4, which is above the critical Reynolds number 11,000 to ensure a flow pattern in the Reynolds number independent regime [17].

In the wind tunnel experiment ethane tracer gas was delivered to the model stack of 2 mm inner diameter at a constant rate via a flowmeter. The emission rate was set at 0.3 l/min for both the isolated building cases and the urban intersection cases, and 0.6 l/min or the cube array cases. A preliminary wind-tunnel investigation was carried out to ensure the released plume was passive [10]. Samples of tracer gas were collected from receptors as shown in Figures 1–3 using 1 mm brass taps fitted either on a rake,

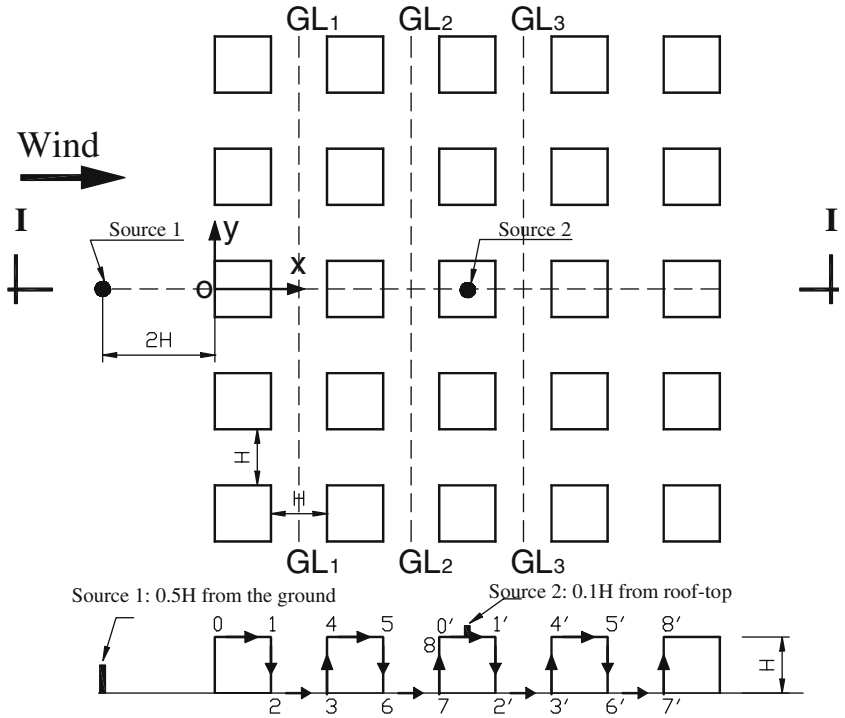

Section I-I 0-8 for sampling line **A1** and 0'-8' for sampling line **A2**

Figure 2. Model, receptors and coordinate system for the cube array case (GL_1, GL_2 and GL_3 are sampling lines on the floor).

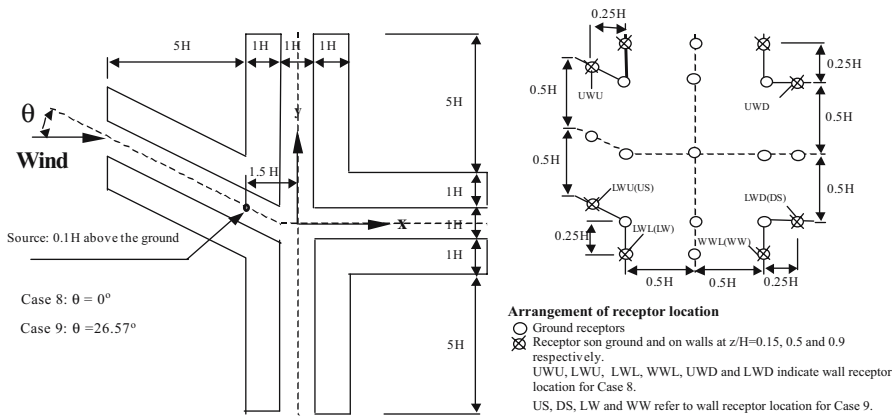

Figure 3. Model, receptors and coordinate system for the urban intersection case.

Table I. Summary of case details ($H = 0.3$ m for case 4 and $H = H_{ref} = 0.1$ m for all other cases).

Case		Model details	Source details
1	Isolated rectangular building	Cube	The stack, $0.5H_{ref}$ high, was installed at an upwind distance of $2H_{ref}$ from the building.
2		$W/H = 2, L/H = 1$	
3		$W/H = 1, L/H = 2$	
4		$W/H = 1/3, L/H = 1/3$	
5		$W/H = 6, L/H = 1$	
6	5 by 5 cube array with in-line arrangement	Plan density 25%	Same as above
7			The stack, $0.1H$ above roof level, was installed at the centre of the middle cube.
8	Urban intersection	Four orthogonal street segments, each street segment was $5H$ long and $1H$ wide	Ground-level source, $0.1H$ high, was located at the centreline of the upwind street at 1H from the edge of the intersection.
9		Upwind street was at an oblique angle of 26.57° to the lateral street, others streets are the same as Case 8.	Ground-level source, $0.1H$ high, was located at the centreline of the upwind street at $1H$ along-wind distance from the edge of the intersection.

model surfaces, or on the raised wind tunnel floor, and concentrations were analysed by a M200 Micro Gas Chromatograph (GC). Plastic tubes were attached to each of the brass taps and connected to a port of a Scanivalve. A user-developed program was used to automatically move the Scanivalve one port forward when a sample had been analysed by the GC. An air pump, which was installed close to the sample inlet of the GC, was used to draw and feed gaseous samples to the inlet of the GC. In this way concentration samples were continuously acquired and analysed by one GC. The corresponding chromatograms and concentration quantities were recorded using a PC. Background concentrations were also measured at the start and end of each sampling session and subtracted from the measured data by presuming that they vary linearly with time.

Measured mean concentrations are expressed as dimensionless C_0-values which are defined as:

$$C_0 = C U_{ref} H_{ref}^2 / Q \tag{13}$$

where U_{ref} and H_{ref} are the reference wind velocity and reference height as given previously, Q is the emission rate and C is the concentration from the GC.

It is worth noting that C_0-values were obtained in terms of the ensemble average of three repeated runs. This is based on the fact that the concentration values from the GC correspond to an average time of only 0.1 s (the injection time of the GC). This ensemble averaging was expected to average out some of the concentration fluctuations from large eddies.

3.3. CFD RUN

The commercially available CFD code, CFX5.6, was used for this evaluation and run on the SGI parallel mainframe at NUI, Galway. CFX5.6 applies a finite volume discretisation scheme on the governing equations of flow quantities in conjunction with an unstructured tetrahedral grid formation, which supplies a number of optional turbulence models, including the standard k–ε (and its RNG modification), k–ω based turbulence model and the Reynolds stress model. This leads to it being an ideal tool to serve for this evaluation.

Based on the set-up used in the wind-tunnel experiment, the computational domain was selected as $H_d \times W_d \times L_d = 1.2 \times 1.9 \times 3.4$ m. This ensures that, for all cases investigated, the inlet boundary was placed upwind of the frontal edge of model buildings by at least $6H$, the outlet boundary was placed downwind of model buildings by at least $15H$, lateral boundaries were placed at least $3H$ from model buildings and the upper boundary was placed $11.5H$ from the top of the model stack. All fluid boundaries were placed far enough away from the models investigated such that the undisturbed flow state was satisfied. Therefore, Dirichlet-type boundary condition for the undisturbed approaching flow was applied to the inlet boundary, zero pressure gradient condition to the outlet, symmetry planes to both lateral surfaces and the upper surface, and no-slip smooth wall conditions to all solid wall surfaces. It is noted that the selection of the large distance for the upper boundary from the models, i.e. $11.5H$, was to ensure the condition of zero pollutant flux could be imposed on the upper boundary.

The Dirichlet-type inlet conditions used in the standard k–ε and the SST models were determined by a combination of measured mean velocity and turbulence intensity profiles with scaled ESDU full-scale data [14, 15]. They are given by:

$$U(z) = U_{\text{ref}}\,(z/H_{\text{ref}})^{\alpha}, \quad k = 0.5\left(\sigma_u^2 + \sigma_v^2 + \sigma_w^2\right), \quad \text{and} \quad \varepsilon = (u_*)^3/(\kappa z), \tag{14}$$

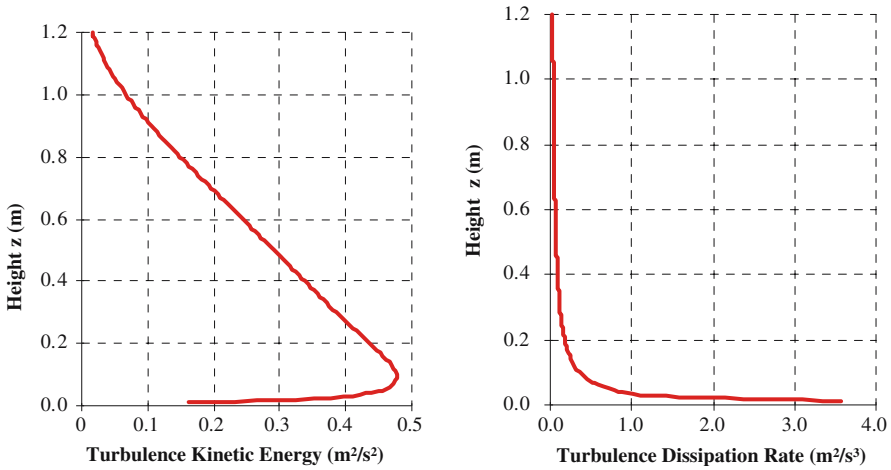

Figure 4. Profiles of k and ε for the inlet boundary condition in CFD calculations.

where parameters $\kappa = 0.4, u_* = 0.245\,\text{m/s}$, $\alpha = 0.256, U_{\text{ref}} = 2.66\,\text{m/s}$ and $H_{\text{ref}} = 0.1\,\text{m}$ are defined previously, σ_u, σ_v and σ_w are the standard deviations of the fluctuating components u, v and w, respectively. The resulting profiles of turbulence kinetic energy, k, and turbulence dissipation rate, ε, are shown in Figure 4.

For the SSG model, the profiles of mean flow, isotropic Reynolds stress components, $\overline{u_i' u_i'}$ and ε in the inlet are identical to Equation (14). The anisotropic Reynolds stress components, $\overline{u_i' u_j'} (i \neq j)$, are approximated by:

$$\overline{u'w'} = -u_*^2 (1 - z/\delta)^2 \quad \text{and} \quad \overline{u'v'} = \overline{v'w'} = 0 \tag{15}$$

where δ is the thickness of the wind-tunnel boundary layer and the expression for $\overline{u'w'}$ is from ESDU [14].

Single neutral tracer gas, (Ethane), was released at an emission velocity of $u_s = 2.0\,\text{m/s}$. The emission velocity is less than the horizontal wind velocity at stack height, i.e. 2.23 m/s, which can be obtained according to the power-law with an exponent of 0.256 and $U_{\text{ref}} = 2.66\,\text{m/s}$, so that meets the requirement of a passive plume condition. This leads that the computational results can be compared with wind tunnel data. For each case investigated, the location of the point source was the same as that in the wind-tunnel experiment (see Table I).

The grid size used in this simulation was at first estimated according to about 100 times the Kolmogorov length scale η which is related to the ε-profile given in Figure 4. From this process, the grid size used in this simulation should not be larger than about 13 mm at the near wall region and 45 mm at a height of 1.2 m above the ground. A further finer mesh size, i.e. 5 mm, was arranged on building surfaces and was expanded gradually

Table II. Details of mesh generation.

Maximum mesh edge length	45 mm
Maximum angle resolution for stack	18°
Surface mesh control	13 mm on ground and 5 mm on building surfaces, effect range = 0, expansion factor = 1.2.
Inflation elements	First layer thickness of 5 mm, 5 layer, expansion factor 1.2

away from the building surfaces. Furthermore an even denser mesh size was used along the normal direction in order to capture the high variation of the mean velocity gradient near the wall area. The schemes for mesh generation are outlined in Table II. Typically, the mesh size is about 1 mm thick near solid surfaces and the maximum length is 45 mm.

High resolution scheme was used for all convection terms of the governing equation. The discretised equations were solved using a built-in coupled algebraic multi-grid solver. Solution convergence was controlled by: (i) the normalised root mean square residuals should be below 1.0×10^{-4}, nd (ii) the global imbalance should be below 5% for all variables.

4. Results and Discussions

In the following evaluation, computed concentrations from the RANS simulation are compared with measured values in wind-tunnel experiments. The coordinate system and the location of both source and receptors in both wind-tunnel experiments and CFD simulation are shown in Figures 1–3. It should be noted that measured lateral concentration profiles used in this evaluation were obtained by averaging measured concentrations in the symmetrical receptors about the centerline, because the original lateral concentration profile was very sensitive to a minor variation of source location from the centerline and thus may be visually asymmetrical.

Detailed flow field simulations are presented in the original work [10]. In order to explain the dispersion phenomena easily, the performance of the three RANS turbulence models, i.e. the standard k–ε, Shear Stress Transport (SST) and the SSG models, in reproducing reattachment lengths around a cube are given as follows [18]:

(i) The three RANS turbulence models exhibited almost identical abilities to predict the stagnation point on the windward wall but predicted different reattachment lengths.

(ii) The standard k–ε model predicted the wake reattachment length well but gave a relatively small upwind ground separation distance. It also failed to predict roof-top flow separation.

(iii) The SST turbulence model predicted roof-top flow separation well and also upwind separation distance but tends to over-predict the wake reattachment length.

(iv) The SSG model predicted roof-top reattachment length well but significantly under-predicted the upwind ground separation distance and over-predicted the wake reattachment length.

CFD simulations of flow fields for both cube array cases and urban intersection cases were also conducted in the original work. Specified flow patterns mentioned in the following analysis, are given in greater detail in references [4, 10, 18].

4.1. ISOLATED BUILDING CASES

For Case 1, the RANS simulations were conducted using three turbulence models respectively. In this simulation, the Reynolds-stress turbulence model failed to converge to the specified criterion, thus the results are only for reference.

Comparisons of the computed near wake concentrations with measured values are given in Figure 5 for Case 1. It is seen that, except for the SST model, the standard k–ε and the SSG model under-predicted near wake concentrations, but all three turbulence models tend to under-predict plume spread. Flow visualization showed that, when the source was placed just ahead of the upwind cavity, the plume separated into three parts [10]: one part of the plume which was above the stagnation point flowed over the obstacle roof, one part passed around the sidewalls and a considerable amount of plume was captured by the horseshoe vortex and

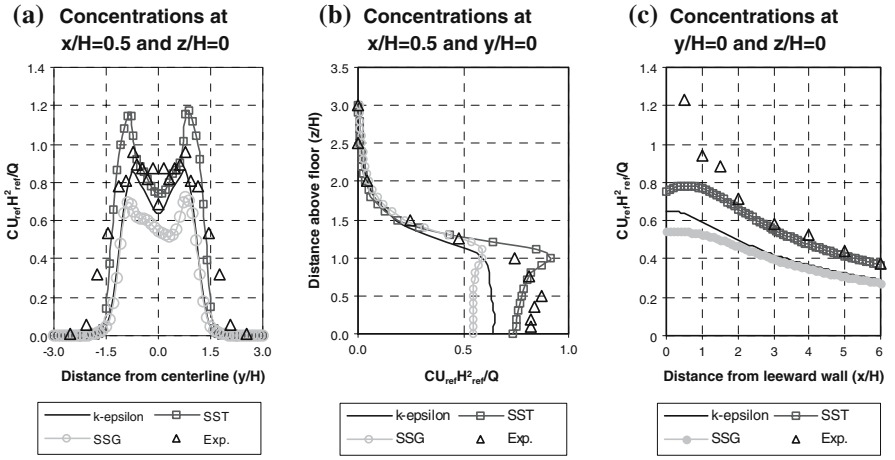

Figure 5. Comparisons of computed with measured concentrations for the case 1 (Cube case).

was kept close to the ground. Therefore, the SST model predicted better near wake ground-level concentrations due to good performance in predicting the upwind cavity length (Figure 5a). On the other hand, the three turbulence models presented almost identical ability to predict the stagnation point, this leads to good agreement between computed and measured concentrations above roof level (Figure 5b). It is obvious that all three turbulence models cannot give a good prediction for receptors close to the cube but agree well with the wind tunnel results farther downwind and above the roof. As shown in Figure 5c, all three turbulence models significantly under-predicted centerline concentrations in the near wake by up to a factor of 2. This is possible due to the larger vortices in the near wake being inherently inconsistent with isotropic turbulence mixing in eddy-diffusivity assumption, but the larger vortices are broken into smaller vortices farther downwind.

It is important to note from the evaluation of Case 1 that, concentrations at specified receptors can be affected by all flow patterns which the plume experienced rather than by the local flow pattern and turbulence characteristics only. This means that the magnitude of prediction errors depend on the turbulence model used and also on receptor locations. For the cube case, the performances of the three turbulence models rank as follows: (1) the SST model, (2) the k–ε model and (3) the RSM model. This has been attributed to better prediction of the part of the plume captured by the horseshoe vortices using the SST model as discussed previously [10]. However, the flow pattern which dominants the plume dispersion around a building could change with its geometry. This leads to further evaluations of the SST model for different building aspect ratios. In addition, another reason for further evaluation was because little information on the application of the SST model in predicting plume dispersion in urban environments can be found in published literature.

Comparisons of the computed near wake concentrations with measured ones, for a wide building (Case 2) and a long building (Case 3) are given in Figures 6 and 7. It was found from these results that the SST models are in general agreement with observations from wind tunnel measurements. Similar to Case 1, it is obvious that the SST model tended to under-predict the plume spread. In contrast to Case 1, however, the SST model tended to over-predict the centerline concentrations for either a wide or a long building (see Figures 6b and 7b). Furthermore, Figures 6c and 7c also shows that computed concentrations for the vertical profiles are higher than measured ones when above the roof level. This suggests that the SST model may over-predict the fraction of plume which passed over the roof-top for either a wide building or a long building.

For a tower-like building (Case 4) or a very wide building (Case 5), prediction errors from the SST model become considerably larger as shown

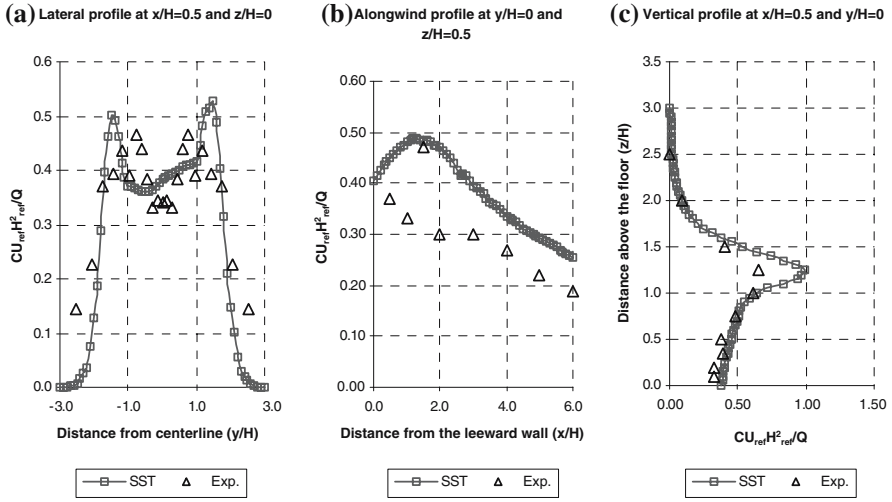

Figure 6. Comparisons of computed with measured concentrations for the case 2 ($W/H = 2, L/H = 1$).

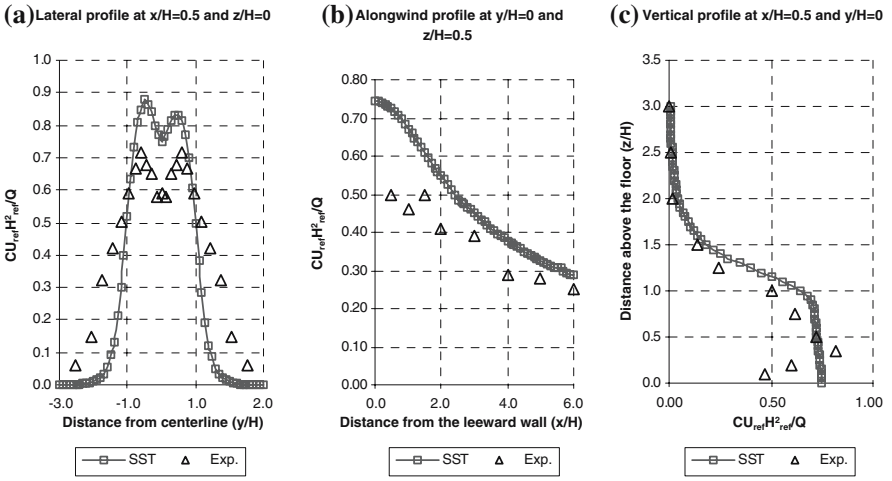

Figure 7. Comparisons of computed with measured concentrations for the case 3 ($W/H = 1, L/H = 2$).

in Figures 8 and 9. For the tower-like building, it is observed that the SST model over-estimated near-wake concentrations substantially (Figure 8). Since the plume cannot pass over a tower-like obstacle directly, the dominant flow patterns for near-wake concentrations close to the ground are the horseshoe vortex and the wake vortex system. In this situation, the computed concentrations at ground level were higher than the measured values (see Figure 8a and b). It was also found that the SST model resulted

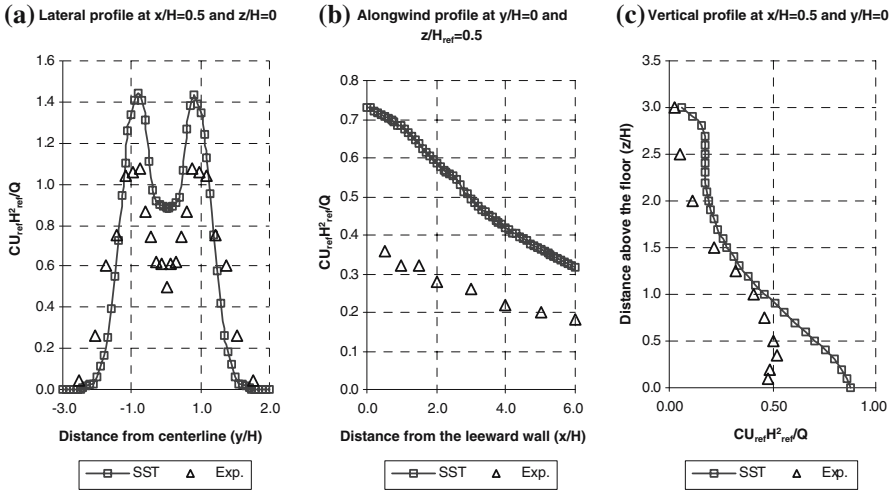

Figure 8. Comparisons of computed with measured concentrations for the case 4 ($W/H = 1/3, L/H = 1/3$).

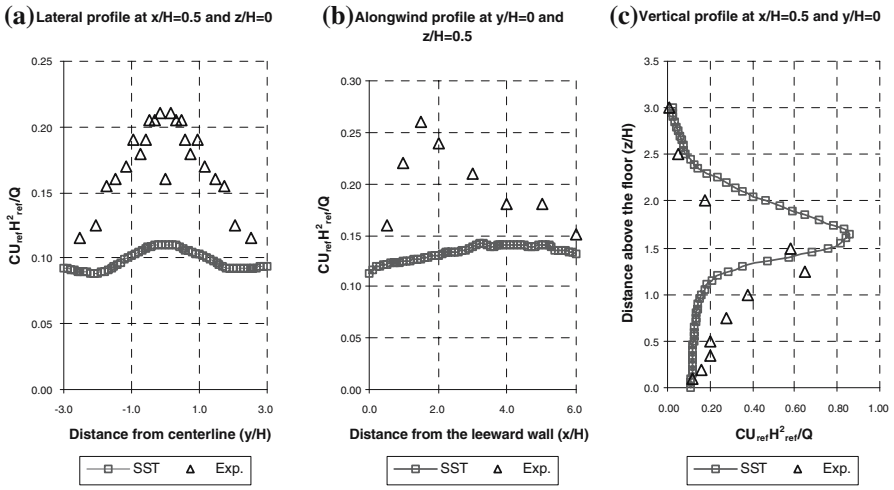

Figure 9. Comparisons of computed with measured concentrations for the case 5 ($W/H = 6, L/H = 1$).

in stronger vertical mass mixing in the near wake because the computed concentrations in the vertical profile were larger relative to measured ones (see Figure 8c). For the very wide building, the influence of the horseshoe vortex on near wake concentrations is negligible since plume bifurcation disappeared (Figure 9a). As a result, almost the entire plume passed over the roof. In this situation, it was found that the SST model considerably over-estimated the height of the plume center downwind of the building

due to over-prediction of the near wake cavity (Figure 9c). Thus predicted concentrations close to the ground were much lower when compared with wind-tunnel observations (see Figure 9a and b).

4.2. CUBE ARRAY CASES

From the evaluations of the isolated building cases, it is known that the prediction of concentrations at specific receptors may depend on mean wind and turbulence characteristic either globally or locally. In other words, the performance of different turbulence models could be changed with variations of the source location and building configurations. For Case 6 (upwind source 1), investigation of flow fields showed that both the k–ε model and the SST model over-predicted the velocity deficit within the cube array, the SST model performs worse [10]. The over-prediction of velocity deficit means that the computed concentrations may be higher than measured ones. As a result, it is obvious from Figures 10 and 11 that the computed concentrations are higher at receptors along lines A_1, GL_1, GL_2 and GL_3 when compared with the measured ones. The standard k–ε model over-predicted the rooftop concentration on the first cube (see Figures 10) but predicted concentrations very well within the cube gaps and also the rooftop concentrations at the remaining downwind cubes (see Figures 10 and 11). The SST model significantly over-predicted concentrations at all locations, by a factor of 2 for the rooftop concentrations (see Figure 10) and by about 65% for the ground-level concentrations (see Figure 11).

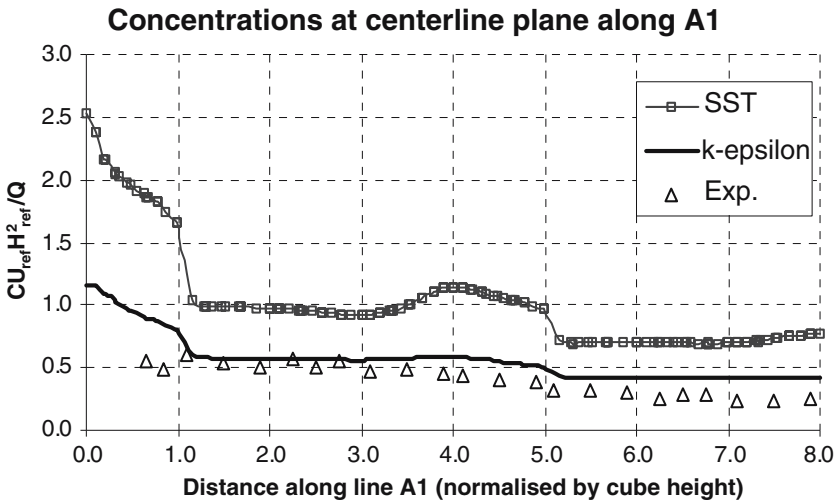

Figure 10. Computed vs measured concentration along A1 for Case 6 (upwind source).

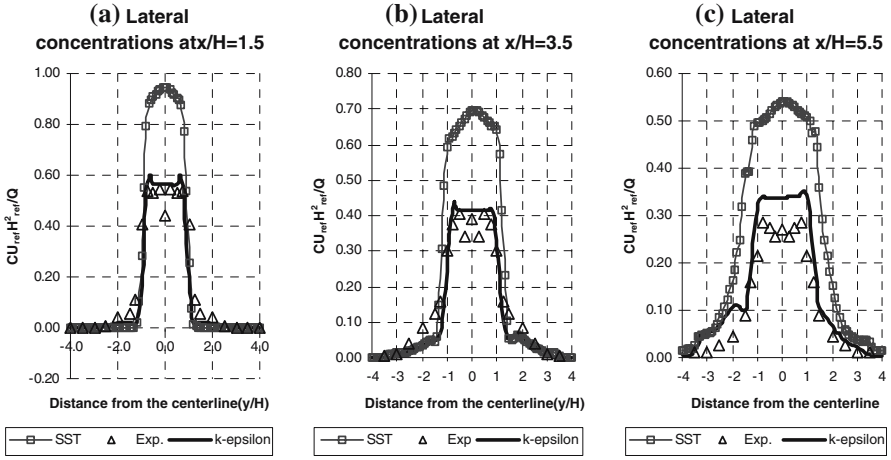

Figure 11. Computed vs measured concentrations along receptor GL_1, GL_2 and GL_3 for Case 6 (upwind source).

For Case 7 (roof source 2), the computed concentrations are significantly higher than the measured ones. The computed peak ground-level concentrations along receptor GL_3 are 2.3 times higher than the measured ones for the k–ε model and 2.5 times for the SST model (see Figure 12a). Significant differences appear along receptor A_2. The SST approach may over-predict ground-level concentration by up to a factor of 10 (see Figure 12b). Although other possibilities exist to cause prediction errors, e.g. experiment error or under-prediction of the mean velocity deficits in CFD, however, they are not strong enough to result in such large errors. Therefore, a reasonable explanation is that the errors are caused mainly from the inconsistencies of 'local mixing' in the eddy-diffusivity assumption, because the vortices between buildings are ejected out and injected into these areas intermittently.

4.3. URBAN INTERSECTION CASES

Evaluation of the standard k–ε model was also extended to urban intersection areas, in which complicated vortex systems could be induced and the flow flux exchange between streets are sensitive to the orientation of the upwind street [19]. Similar to Case 7, for traffic emissions in the vicinity of intersections, due to the intermittent flow exchange between in-canyon flow and roof-top wind the simple eddy-diffusivity assumption may be inherently inconsistent with realistic pollutant dispersion. Furthermore, wall functions used in the RANS scheme may lead to incorrect simulation of near-wall turbulence characteristics. Cases 8 and 9 were designed to investigate the resulting prediction errors.

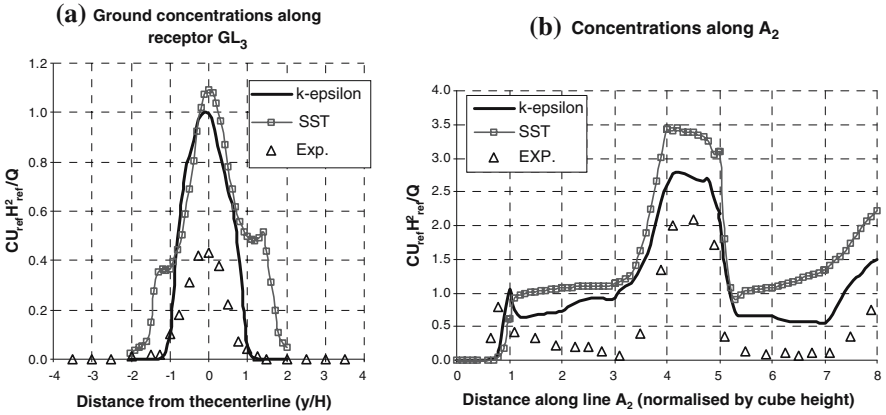

Figure 12. Comparison of computed concentrations with measured ones for Case 7 (roof source).

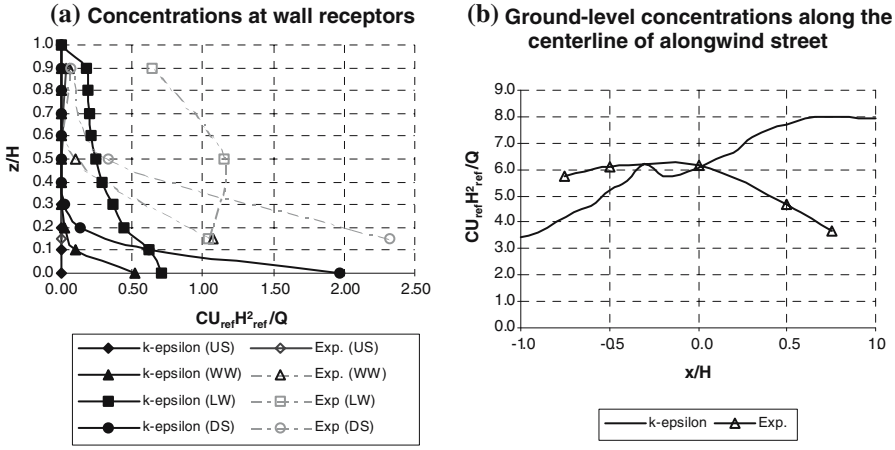

Figure 13. Computed vs measured concentrations for Case 8. US: receptors on walls of the upwind street, WW: receptors on the windward wall of lower lateral street, LW: receptors on the leeward wall of the lower lateral street, DS: receptors on walls of the downwind street.

For the orthogonal intersection (Case 8), Figure 13a shows that, in comparison with computed concentrations, the measured concentrations were significantly higher at wall receptors of the downwind street, but become lower for ground-level receptors along the centerline when $x/H > 0$ (see Figure 13b). This demonstrates that the plume spread in the wind-tunnel experiment was much larger than that in the CFD simulation. Furthermore, Figure 13b shows that the larger plume spread in the wind-tunnel experiment was caused possibly by the higher release velocity since measured concentrations were lower than computed ones at ground-level receptors along the centerline when $x/H < 0$. Therefore, this

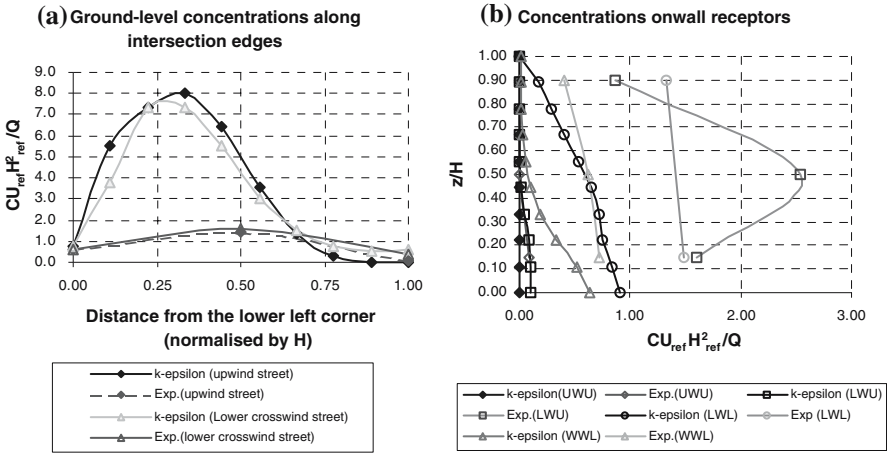

Figure 14. Comparisons of computed with measured pollutant concentrations for the irregular intersection. UWU: receptors on the upper-side wall of the upwind street LWU: receptors on the lower-side wall of the upwind street. LWL: receptors on the windward wall of lower lateral street; WWL: receptors on the leeward wall of the lower lateral street.

suggests that the k–ε model under-predicted flux exchange by corner vortices between alongwind streets and lateral streets at the intersection. This also resulted in the computed concentrations at wall receptors of the lateral streets being much smaller than the measured ones although they show a similar distribution on both windward and leeward walls (see Figure 13a).

For the intersection with an oblique upwind street (case 9), as shown in Figure 14, the computed concentrations show similar trends as those in the orthogonal intersection, i.e. significant underestimation of plume spreading and the mixing ability of the corner vortex. It is clear from Figure 14a that the computed ground-level concentrations along intersection edges are much lower than measured values. It can also be seen from Figure 14b that the prediction errors increased significantly at wall receptors on the upwind street wall in the vicinity of the lower left corner, in which computed concentrations are lower than measured values by up to a factor of 10. This shows that the standard k–ε failed to predict the concentration distribution completely in this case.

5. Summary and Conclusions

By comparing computed concentrations using RANS methods with values from wind-tunnel experiments at specified receptors, a series of evaluations have been carried out to examine the applicability of the RANS methods in simulating pollutant dispersion in typical urban environments. The evaluations are summarized as follows:

(1) For emission from an upwind low-level source near a cubic building, all three RANS turbulence models, i.e. the standard k–ε model, the SST model and the SSG model tend to under-estimate the near-wake concentrations. The SSG model was sensitive to grid density and may lead to difficulty in convergence and thus was not used in practical applications. The predicted near-wake concentrations using the standard k–ε model were in general agreement with measured values. The SST model performed best in this case.

(2) An extended evaluation was then conducted for the SST model for the isolated building cases with different aspect ratios. The SST model predicted near-wake concentrations better for a wide and a long building. The prediction error became considerably larger for a tower-like building; it over-predicted vertical turbulence mixing giving higher concentration distributions vertically. For a very wide building, the SST model failed to predict the correct concentration distribution in the near wake. The over-prediction of plume elevation led to the computed near-wake concentrations being lower than the measured values by up to a factor of 2.

(3) Both the standard k–ε model and the SST model were evaluated for emissions from an upwind low-level source and from a roof-top source in the cube array case. For the upwind low source, the SST model significantly over-estimated concentrations within the cube array, but the standard k–ε gave good predictions. For the roof-top source, both turbulence models substantially over-predicted concentrations at the same receptors.

(4) The evaluation of the RANS methods was only conducted for the standard k–ε model in urban intersection cases, because it has been verified from the evaluation of the cube array cases that the SST model performed worse when channeling flow and in-canyon vortices dominate a dispersion process of pollutants. For the orthogonal intersection case, the standard k–ε model under-predicted flux exchange by corner vortices between alongwind streets and crosswind streets, the computed concentrations at wall receptors of crosswind streets were much lower than measured ones. For the oblique upwind street case, the prediction errors became very large, and thus no concentration distribution of reasonable accuracy was obtained.

Therefore, it is clear from this evaluation that there does not exist a turbulence model superior to others, among those tested here, in all cases investigated. Generally speaking, the RANS methods can lead to significant prediction error in the following situations:

a. Inappropriate reproduction of the most important mean flow pattern which dominates the dispersion process, e.g. the horseshoe vortex for

the isolated building cases. However, better results may be obtained by selecting a suitable turbulence model.

b. Inappropriate description of 'non-local' high turbulence mixing. For example, neither the standard k–ε nor the SST models can correctly predict the ground-level concentrations when the plume passes directly over a cube array. This is because intermittent flow ejection out of and injection into gaps leads to turbulent mixing being no longer 'local'. In this situation, the large error can not be overcome by selecting a suitable turbulence model only.

c. Inappropriate modelling of wall turbulence also causes prediction error to some extent. This may be an error source causing significant under-prediction of plume spreading for the intersection case, since the ground-level source is directly affected by wall turbulence.

Acknowledgements

This work was sponsored by a grant from the HEA of Ireland No: ECI: WA-3. The authors would like to thank the National Centre for Biomedical Engineering Science at NUI, Galway, for providing the computational resources for this study.

References

1. Zhang, Y.Q., Arya, S.P. and Snyder, W.H.: 1996, A comparison of numerical and physical modeling of stable atmospheric flow and dispersion around a cubical building, *Atmos. Environ.* **30**, 1327–1345.
2. Sini, J.-F., Anquetin, S. and Mestrayer, P.G.: 1996, Pollutant dispersion and thermal effects in urban street canyons, *Atmos. Environ.* **30**, 2659–2677.
3. Chan, A.T., So, E.S.P. and Samad, S.C.: 2001, Strategic guidelines for street canyon geometry to achieve sustainable street air quality, *Atmos. Environ.* **35**, 4089–4098.
4. Wang, X. and McNamara, K.F.: 2002, CFD simulation of plume dispersion within clusters of buildings. In: *Proceedings of the 5th UK Conference on Wind Engineering*, Nottingham, UK, pp. 101–104.
5. Scaperdas, A. and Colvile, R.N.: 1999, Assessing the representativeness of monitoring data from an urban intersection site in central London, UK, *Atmos. Environ.* **33**, 661–674.
6. Meroney, R.N., Leitl, B.M., Rafailidis, S. and Schatzmann, M.: 1999, Wind-tunnel and numerical modeling of flow and dispersion about several building shapes, *J. Wind Eng. Ind. Aerodyn.* **81**, 333–345.
7. Leitl, B.M., Kastner-Klein, P., Rau, M. and Meroney, R.N.: 1997, Concentration and flow distributions in the vicinity of U-shaped buildings: Wind-tunnel and computational data, *J. Wind Eng. Ind. Aerodyn.* **67** & **68**, 745–755.
8. Cowan, I.R., Castro, I.P. and Robins, A.G.: 1997, Numerical considerations for simulations of flow and dispersion around buildings, *J. Wind Eng. Ind. Aerodyn.* **67** & **68**, 535–545.

9. Richards, P.J., Quinn, A.D. and Parker, S.: 2002, A 6 m cube in an atmospheric boundary layer flow Part 2. Computational solutions, *Wind Struct.* **5**(2–4), 177–192.
10. Wang, X.: 2004, Numerical and wind tunnel simulations of building effects on pollutant dispersion, PhD dissertation, National University of Ireland, Galway, Ireland.
11. Rodi, W.: 1993, Turbulence Models and their Application in Hydraulics. A State-of-the-Art Review, third ed., A.A. Balkema, Rotterdam.
12. Murakami, S.: 1997, Current status and future trends in computational wind engineering, *J. Wind Eng. Ind. Aerodyn.* **67** & **68**, 3–34.
13. CFX-international: 2003, CFX version 5.6: User Manual.
14. ESDU: 1983, Strong winds in the atmospheric boundary layer. Part 2: discrete gust speeds. Item No. 83045.
15. ESDU: 1985, Characteristics of atmospheric turbulence near the ground, Part II: single point data for strong winds (neutral atmosphere). ESDU item No. 85020.
16. ESDU: 1982, Strong winds in the atmospheric boundary layer. Part 1: mean-hourly wind speeds, ESDU item No. 82026.
17. ASCE: 1996, Wind tunnel studies of building and structures, *J. Aerospace Eng.* **9**, 19–36.
18. Wang, X. and McNamara, K.F.: 2005, Numerical and wind tunnel simulation of pollutant dispersion in the near wake of buildings, *Wind Struct.* **8**, 427–442.
19. McNamara, K.F and Wang, X.: 2005, Effects of street orientation on dispersion at or near urban street intersections, In: *Proceedings of the 4th European & African Conference on Wind Engineering,* pp. 228–229. Prague, Czech Republic.